UNIVERSIDAD COMPLUTENSE DE MADRID

FACULTAD DE CIENCIAS FÍSICAS

Máster en Astrofísica

TRABAJO DE FIN DE MÁSTER

Conexiones homoclínicas y heteroclínicas en variedades invariantes de las órbitas en torno a sistemas binarios

Homoclinic and heteroclinic connections between invariant manifolds of orbits in binary systems

Payeras Seguí, Jaume

Tutor/es:

Romero Gómez, Mercè

Roca Fàbrega, Santi

Curso académico 2022-23

Contents

Abstract

This work extends the investigation on circumstellar and circumbinary orbits in binary systems done in Jaime et al., 2014 by studying the possibility of existence of such orbits due to homoclinic or heteroclinic connections between the invariant manifolds of the Lyapunov orbits of the collinear libration points of the binary under study.

The binary Kepler 47 is the focus of analysis and many homoclinic and heteroclinic connections are found. One of them is also stable, i.e. does not escape the vicinity of the binary through an unstable manifold from either the L_1 or L_3 Lyapunovs. In particular that orbit is a circumstellar that surrounds m_1, the larger primary. It is seen that this orbit can collapse with the primary but for other energies or initial conditions there might be orbits of that kind that do not collapse with the principal.

Overall it can be confirmed that homoclinic and heteroclinic orbits are present in this type of stellar system and that they can also constitute stable paths where, if the relative distances allow to it, planetary formation could occur.

En este trabajo se extiende la investigación de órbitas circumestelares y circumbinarias en sistemas binarios de estrellas del artículo Jaime et al., 2014 estudiando la posibilidad de existencia de esos tipos de órbitas debido a conexiones homoclínicas o heteroclínicas entre las variedades invariantes de las órbitas Lyapunov de los puntos de equilibrio colineales de la binaria bajo estudio.

La binaria Kepler 47 es el foco de análisis y varias órbitas homoclínicas y heteroclínicas son halladas. Una de ellas es estable, es decir, al evolucionar en el tiempo se mantiene próxima al sistema binario y no escapa del mismo a traves de las variedades invariantes inestables de las Lyapunov de L_1 *o* L_3*. La órbita en cuestión es una circumestelar que orbita* m_1*, el primario mayor. Se puede ver como esta órbita colapsa con el mismo pero para otras energías o condiciones iniciales podrían existir orbitas de este tipo que no colapsaran.*

Al final se puede confirmar que las órbitas homoclínicas y heteroclínicas están presentes en este tipo de sistema estelar y que, además, pueden constituir trayectorias estables y confinadas en una región próxima a la binaria en las que, si las distancias relativas entre los primarios lo permiten, puede llegar a darse formación planetaria.

1 Objectives

The objective of this work is to extend the research of Pichardo et al., 2005 and Jaime et al., 2014 on the stability of orbits around stellar binaries. There, periodic circumbinary and circumstellar orbits called *invariant loops* are studied as possible bound orbits where planetary formation can happen. These *invariant loops* are closed curves such that particles that begin their orbit on them after each binary period return to their same initial position on the curve. Each position on this curve will have a different orbit associated but will always return to the same *invariant loop* after the binary period.

This work assesses this search of bound orbits from a different perspective, that is, analysing whether the **invariant manifold orbits** from the *libration points* of the binary system can sustain **heteroclinic** or **homoclinic connections** in order to constitute other circumbinary and circumstellar orbits **where planetary formation can occur**.

In particular, one stellar binary of those studied in Jaime et al., 2014 is chosen to have almost circular orbits around their centre of mass (i.e. that have very low excentricity and the *Planar Circular Restricted Three Body Problem* can be applied) and will be the focus of our study, namely to check those connections among the different branches of their invariant manifolds. This binary is: **Kepler 47**.

The first objective of the study is to find these types of connections among the invariant manifolds of Kepler 47 and, if found any possible trajectory of this kind and remains bound to the vicinities of the binary, it would also be possible to **give coordinates around binaries for observers to look for possible exoplanets**.

2 Theoretical Background

As already mentioned in the Objectives (section 1), the aim of this work is to study the orbits in the invariant manifolds and find possible heteroclinic or homoclinic connections. For this reason, in this section, a brief explanation on the physics applicable in this dynamic system will be presented based on acknowledged literature on this matter as Szebehely, 1967, Koon et al., 2011 and Romero-Gómez et al., 2006.

Since the dynamical system is formed by three particles that are only affected by their mutual gravitational influence, the basic equation that needs to be considered here is that of Newton's universal law of gravitation. Therefore, the problem in hand could be approached using the **General Three Body Problem** but in this work there is one reduction to the problem that can be done based on the hypothesis that one of the three particles of the system has far significantly less mass than the others. This implies that its influence on the other two main bodies can be neglected in the equations of motion.

In this case the hypothesis is valid since the third body is meant to be a planet or the gas and minor solid particles that conform the planetary formation discs and any of them have much lower mass than the binary stars.

Because of this, the problem will be approached as a **Restricted Three Body Problem**. More specifically, the problem in hand is also restricted to the orbital plane of the two stars, called *primaries*, and which move in circular motion around each other. That is, to have an autonomous or time-invariant Hamiltonian (Szebehely, 1967) so that the problem depends only on one parameter, the parameter of masses μ, which is the relation of the smaller primary to the total mass, and it constitutes an integral of motion. For these reasons, the problem can also be named as the **Planar**

Circular Restricted Three Body Problem, or **PCR3BP** for short.

This approximation will be used to study the orbits around stellar binaries but it can be applicable to any dynamical system with two main bodies and other with negligible mass. For this reason, in Koon et al., 2011 and Koon et al., 2000 the **PCR3BP** is used in the environment of the Solar System to study possible trajectories of spacecrafts and actual trajectories of asteroids or comets, more in particular of the Trojans of Jupiter. For example, the observed orbit for the Jupiter comet *Oterma* is seen to match an orbit computed with homoclinic and heteroclinic connections among the different invariant manifolds of L_1 and L_2 of Jupiter. In the field of astrophysics, the connections among invariant manifolds are also used to find trajectories of material transportation in barred galaxies, where the potential field also gives rise to equilibriumm points with the collinear points placed along the major axis of the bar and being the extremal gates of material exchange between the interior of the bar and the rest of the galaxy, as is studied in Romero-Gómez et al., 2006 and Romero-Gomez et al., 2007.

The motion of the two primaries can be simply described as circular orbits in a Two Body Problem, therefore being two masses that impose a rotating gravitational field upon their surroundings. Figure 1 represents the system.

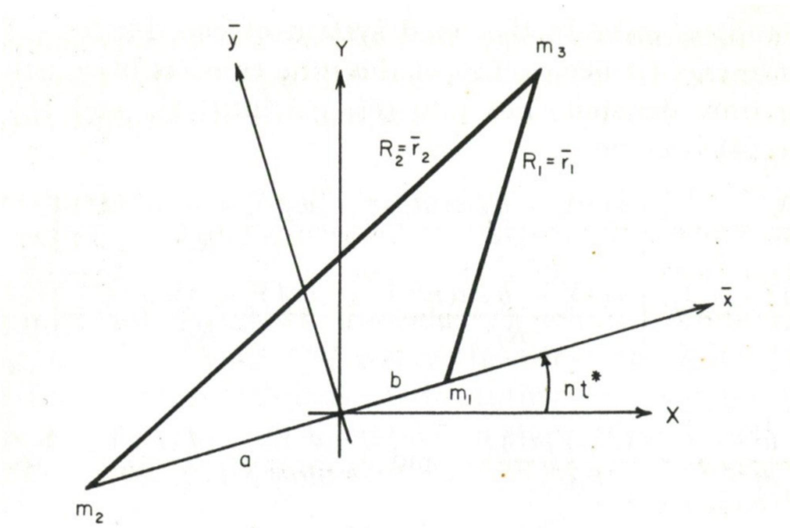

Figure 1: The inertial (sidereal, (X, Y)) and the rotating (synodic, $(\tilde{x}, \tilde{y})$ coordinate systems $(m_1 > m_2 >> m_3)$ (Szebehely, 1967).

In Figure 1 the coordinates of the inertial (sidereal) frame are X and Y while those of the rotating (synodic) frame are $\tilde{x}$ and $\tilde{y}$. Note that time is represented by t^* and the mean motion by n, therefore the two primaries rotate at a fixed rate nt^*.

The equations of motion of the third body in the inertial frame are explicitly time dependent due to the circular motion of the principal bodies. This, due to the approximation inherent in the restricted problem, causes the energy not to be conserved. For this matter, the rotational frame is used since in it the time dependence vanishes and the called **Jacobian integral** becomes an integral of motion.

Therefore, the **equations of motion** of the third body in the rotating frame and after making the problem dimensionless are:

$$\begin{aligned} \ddot{x} - 2\dot{y} &= \Omega_x \\ \ddot{y} + 2\dot{x} &= \Omega_y \end{aligned} \tag{1}$$

where the dots represent time derivatives, the subscripts spacial derivatives and the variables are made **dimensionless** by:

$$x = \frac{\tilde{x}}{l}, \quad y = \frac{\tilde{y}}{l}, \quad t = nt^*, \quad r_1 = \frac{\tilde{r}_1}{l}, \quad r_2 = \frac{\tilde{r}_2}{l}, \quad \mu_{1,2} = \frac{m_{1,2}}{M} \tag{2}$$

where x and y are the dimensionless coordinates of the rotating frame, l is the distance between the primaries, t the dimensionless time (although is actually a measure of the binary star's period), r_1 and r_2 the distances from each primary to the third body, $\mu_{1,2}$ the mass parameters of each primary and M the total mass of the two primaries. Since via dimensionalization the problem has been scaled to $\mu_1 + \mu_2 = 1$ then there is only one mass parameter that is independent, thus $\mu_2 = \mu$ and $\mu_1 = 1 - \mu$ are used. Here the selection of the distance, time and mass units have been done such that the length between the primaries is unity, the sum of their masses is also unity, the graviational constant G is unity and the mean motion n is unity. For each value of mass parameter these unit values will be different.

In equation 1 the Ω represents the *negative effective potential* which is the potential as seen from the rotating frame since it includes the effects of the centrifugal force and the gravitational potential. This **effective potential** is of the form:

$$\Omega = \frac{1}{2}(x^2 + y^2) + \frac{1-\mu}{r_1} + \frac{\mu}{r_2} + \frac{1}{2}\mu(1-\mu) \tag{3}$$

where an additional term to the potential and centrifugal contribution, $\frac{1}{2}\mu(1-\mu)$ is added by convention (Szebehely, 1967 and Koon et al., 2011).

$$\begin{aligned} r_1^2 &= (x-\mu)^2 + y^2 \\ r_2^2 &= (x+1-\mu)^2 + y^2 \end{aligned} \tag{4}$$

From equations 1 an integral of motion can be obtained with different approximations as computing the Hamiltonian (Koon et al., 2011). This integral is named the **Jacobian integral** and is as follows.

$$\frac{1}{2}v^2 = \Omega - \frac{C}{2} \tag{5}$$

where $v^2 = \left(\frac{dx}{dt}\right)^2 + \left(\frac{dy}{dt}\right)^2$ is the velocity of the body. Here, C is the Jacobian constant which can be considered as a measure of the energy of the particle in the rotating frame.

Studying the Jacobian integral, since the left-hand term is always positive, there arises an inequation that restricts the regions, named *Hill's regions*, where a particle with certain energy, i.e. Jacobi constant, can access. The limiting equipotential lines are those with null velocity and that satisfy $\Omega = \frac{C}{2}$. These are called **zero velocity curves** and represent the limits of the motion of the body being it only possible where $\Omega \geq \frac{C}{2}$.

Equations 2 can be rearranged in a system of first order differential equations with $(x, y, \dot{x}, \dot{y}) = (x_1, x_2, x_3, x_4)$ as follows:

$$\begin{aligned} \dot{x_1} &= x_3 \\ \dot{x_2} &= x_4 \\ \dot{x_3} &= 2x_4 + \Omega_x x_1 \\ \dot{x_4} &= -2x_3 + \Omega_y x_2 \end{aligned} \tag{6}$$

This dynamical system, as is well known, has five different **equilibrium points** at different locations that can be found by equating to zero equations 6. From them one can find that three of the equilibrium points, also named **libration points** or **Lagrange points**, are located on the x axis and are named **collinear points** and that the other two are called *equilateral points* because are located forming two different equilateral triangles where the two vertix of the basis are the locations of the primaries. Figure 2 displays the locations of these points and also represents the forbidden regions by the zero velocity curves for different ranges of energy between those of the equilibrium points. See how as the energy increases from a similar value of the L_1 point to that of the equilateral points, the restricted regions decrease making it possible first the transit between primaries (case 2) and then between the outer and inner regions (case 3).

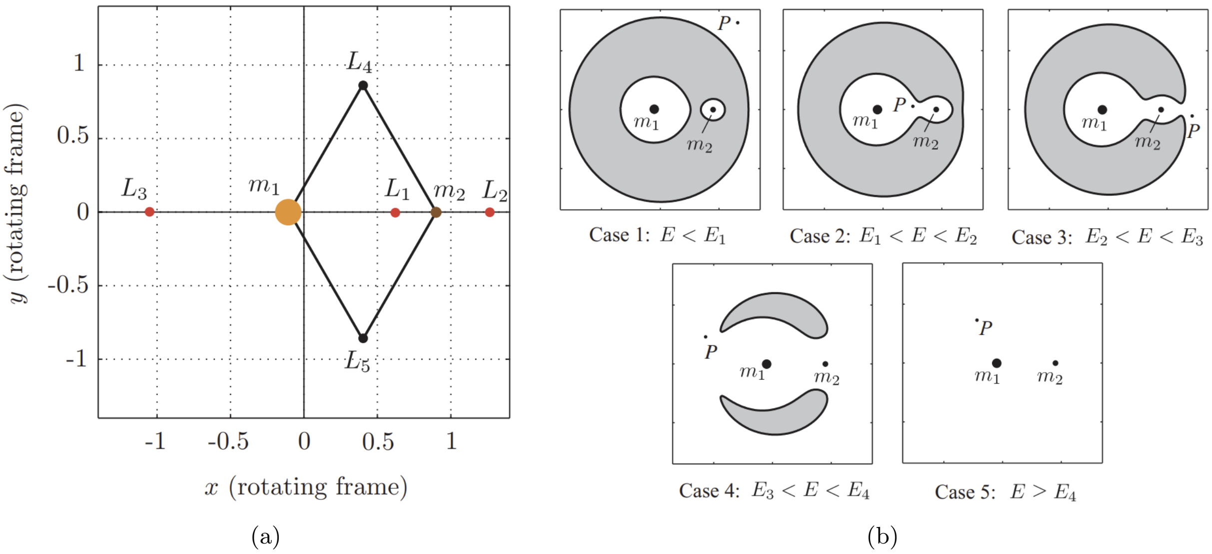

Figure 2: a) Representation of the collinear points L1, L2 and L3 and the equilateral points L4 and L5. b) Representation of the forbidden regions (in grey) for different ranges of energy, from low energies similar to L1 (E_1) to higher ones of L5 ($E_5 = E_4$).(Koon et al., 2011)

For the present work only the collinear points are considered for the study therefore the equilateral points are left aside. Since the present focus is to find the intersections between invariant manifolds, it is necessary to know how these particular regions of the phase space are computed on the first place. For this reason the behavior of the equations of motion in the neighbourhood of the libration points is studied as follows according to Romero-Gómez et al., 2006.

From equations 1, the effective potential can be expanded to the second order and using the following renaming $x \equiv x - x_L$, $y \equiv y - y_L$, meaning that the coordenates now have their origin on the corresponding libration point, the equations result:

$$\begin{aligned} \ddot{x} &= 2\dot{y} + \Omega_{xx}x \\ \ddot{y} &= -2\dot{x} + \Omega_{yy}y \end{aligned} \tag{7}$$

allowing the notation of $\Omega_{xx} = \left(\frac{\delta^2\Omega}{\delta_x^2}\right)_{Li}$ and $\Omega_{yy} = \left(\frac{\delta^2\Omega}{\delta_y^2}\right)_{Li}$. The crossed second derivative terms are null due to symmetry in the potential.

Rearranging equations 7 to first order differential equations as in Equation 6, the system is of the form $\dot{\mathbf{x}} = Df_x\mathbf{x}$ with the differential matrix Df_x as:

$$Df_x = \begin{pmatrix} 0 & 0 & 1 & 0 \\ 0 & 0 & 0 & 1 \\ \Omega_{xx} & 0 & 0 & 2 \\ 0 & \Omega_{yy} & -2 & 0 \end{pmatrix} \tag{8}$$

After solving for the eigenvalues of the matrix, four solutions are found, $\lambda, -\lambda, \omega i, -\omega i$, each of them corresponding to an eigenvector. The solution of the positional coordinates is of the form

(Romero-Gómez et al., 2006):

$$\begin{aligned} x(t) &= X_1e^{\lambda t} + X_2e^{-\lambda t} + X_3cos(\omega t + \phi) \\ y(t) &= A_1X_1e^{\lambda t} - A_1X_2e^{-\lambda t} + A_2X_3cos(\omega t + \phi) \end{aligned} \tag{9}$$

with

$$A_1 = \frac{\Omega_{xx} + \lambda^2}{2\lambda} \qquad A_2 = \frac{\Omega_{xx} - \omega^2}{2\omega} \tag{10}$$

The solutions in Equations 9 behave differently depending on the values of the coefficients of each summand. It is possible to see how if time tends to infinity the term of the positive λ eigenvalue will dominate as the same with the negative λ when time tends to minus infinity. Now, for those orbits with null X_1 and X_2 the above equations become:

$$\begin{aligned} x &= X_3cos(\omega t + \phi) \\ y &= A_2X_3sin(\omega t + \phi) \\ \dot{x} &= -\omega X_3sin(\omega t + \phi) \\ \dot{y} &= \omega A_2X_3cos(\omega t + \phi) \end{aligned} \tag{11}$$

which are the **equations of the Lyapunov orbits**, i.e., the unstable periodic orbits around the libration points. Unstable because any small perturbation, as will be following presented, would set the orbit in one of the asymptotic manifolds which correspond to those orbits with $X_1, X_2 \neq 0$. Those orbits constitute the invariant manifolds that are object of study of this work. An illustration of these type of orbits is shown in Figure 3.

From equations 9, if $X_1 \neq 0$ and $X_2 = 0$ then it can be seen that as time tends to minus infinity the orbit tends to the Lyapunov as the exponential tends to zero, these orbits constitute the unstable invariant manifold of the solutions. For the other case of $X_1 = 0$ and $X_2 \neq 0$, the opposite situation happens, where the orbits tend to the Lyapunov as time tends to infinity and, consequently, constitute the stable invariant manifold. See Figure 3 for visualization.

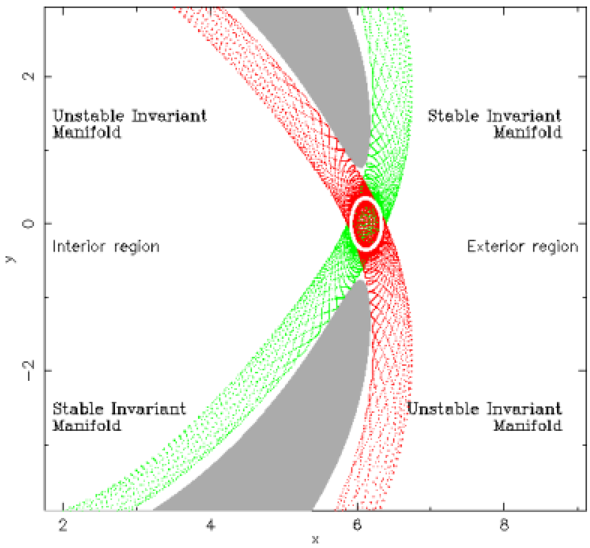

Figure 3: Invariant manifolds. In the intersection of the two manifolds, the Lyapunov orbit is represented as a white circle. The two branches of the unstable invariant manifold (red), and the two branches of the stable invariant manifold (green). In grey, the forbidden region surrounded by the zero velocity curves. Romero-Gómez et al., 2006.

Equations 11 are analytical for the neighbourhood and, although the implications of stability around the libration points can be extended to the non-linear equations of the entire field, they are

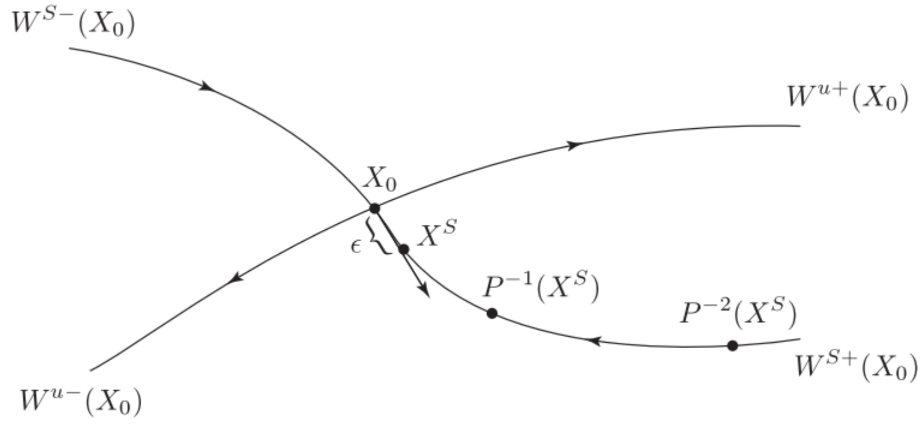

Figure 4: A simple way to compute an approximation of the two branches of the unstable ($W^{u\pm}$) or stable ($W^{s\pm}$) manifolds of a periodic orbit, which appear as manifolds to a fixed point in a Poincaré map P. (Koon et al., 2011).

only used to compute the initial conditions for the numerical integration of the Lyapunov orbits from which the invariant manifolds will also be integrated numerically with other set of initial conditions.

Forwarding to the derivation of the **invariant manifolds**, setting small perturbations on equations 7, the variational equations are obtained on the form of:

$$\dot{\delta} = \frac{\delta \mathbf{f}}{\delta \mathbf{x}_i}\delta = \sum_{i=0}^{6} \frac{\delta f_k}{\delta x_i}\delta_i \tag{12}$$

where $\frac{\delta \mathbf{f}}{\delta \mathbf{x}_i}$ is the *state transition matrix* when is evaluated over a trajectory for a certain initial conditions. This matrix, when used for a periodic trajectory as the Lyapunov orbit and is integrated over one period, is named the **monodromy matrix**. Then, as has been done previously with the differential matrix of the neighbourhoods of the libration points, this matrix can also be used to find the eigenvalues and eigenvectors which give information about the stability of the vicinities of these Lyapunov orbits.

From Koon et al., 2011 it is seen that the **monodromy matrix** has four eigenvalues $\lambda_1 > 1$, $\lambda_2 = \frac{1}{\lambda_1}$ and two unitary eigenvalues. The first two eigenvalues correspond to the unstable and stable invariant manifolds respectively. Figure 4, as with 3, represents these directions of the eigenvectors that depart from or tend to the Lyapunov orbit. The initial condition for the computation of the invariant manifolds can be guessed with:

$$X^i(X_0) = X_0 + \epsilon Y^i(X_0) \tag{13}$$

where i can be S or U meaning stable and unstable branches, ϵ is a small perturbation and Y is the normalized eigenvector. To find the initial condition from another point on the Lyapunov orbit, the *state transition matrix* can be used (Koon et al., 2011):

$$Y^i(X(t)) = \Phi(t,0)Y^i(X_0) \tag{14}$$

with Φ as the *state transition matrix.*

The invariant manifolds, are usually referred to as *tubes* because in the phase space their intersections with **Poincaré maps** of type $\dot{x}, x$ for $y = 0$ and $\dot{y} > 0$, for example, are closed curves. These maps provide important information about the behavior of the orbits as they approach the region close to the libration point. Those orbits that are part of the invariant manifold, that is, that are

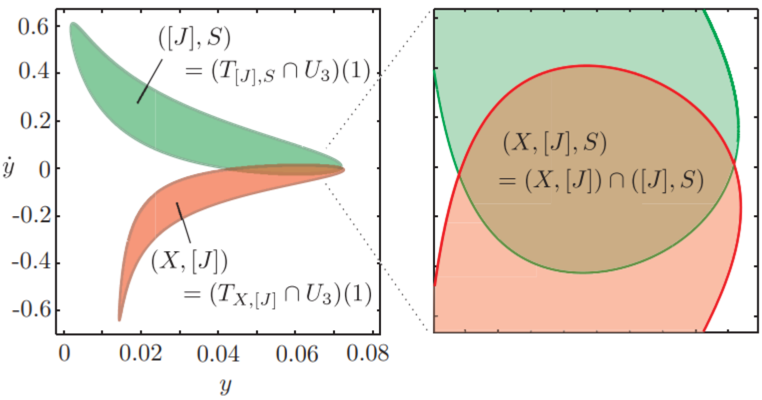

Figure 5: Intersection of the unstable invariant manifold from L_2 of the system Sun-Jupyter and the stable manifold of L_1. As can be seen, there is a region where both overlap, meaning that there are orbits that can be considered from the two manifolds and, consequently, heteroclinic. (Koon et al., 2011)

on the curve itself, will tend, as previously stated, asymptotically to the Lyapunov orbit as time tends to positive or negative infinity depending on whether it is on the stable or unstable branch, respectively. Nonetheless, all the other orbits reside in two different regions, the exterior region of the manifold and the interior region. These two regions have an easily understood behavior when analysing their orbits in the eigenbasis coordinate system from the solution of 8, as seen in Koon et al., 2011. There can be seen how the orbits within the invariant manifolds transit from one side of the libration point neighbourhood to the other, making them *transit orbits*, and the orbits outside the manifold approach the libration point but exits its region returning to the same where it came from, making it a *non-transit orbits.*

The following Figure 5 displays one of these cuts between two different manifolds from **different libration points** with an overlapping region, i.e. with a region in the phase space where exist **heteroclinic orbits**. If they where from the **same manifold**, then the orbits would be **homoclinic**.

It is precisely in the heteroclinic and homoclinic orbits that we are interested in this work. A particle, or in this case a planet, on an heteroclinic or homoclinic orbit will stay there orbiting the two primaries, so becoming bound circumstellar or circumbinary orbits.

3 Methodology

With the theory background settled, the computation of the different invariant manifolds for each of the collinear libration points is adressed with an already tested Fortran code (used in Romero-Gómez et al., 2006 and Romero-Gomez et al., 2007), which assesses the computation of the Lyapunov orbits, the invariant manifolds and their Poincaré maps. This Fortran code is managed by a Python set of scripts that ensure the correct order of execution.

A nominal execution for a specific value of mass parameter (μ) follows these steps:

1. Select a mass parameter, μ.
2. Compute the position of the libration points and their Jacobi constants as presented in Section 2 (Equations 6 and 3) for the selected mass parameter.
3. Compute the Lyapunov orbits around the collinear points for a specific energy finding the

imaginary eigenvalues in Equation 8 and then computing the orbit using a Runge-Kutta 7(8) integration from the initial conditions computed at t_0 with Equation 11 until one period is completed. For this step and the following, the Runge-Kutta 7(8) is computed with a tolerance of $1e-5$ in the energy disparities between the initial and the final energy, to ensure conservation, if the orbit exceeds this difference, it cannot be accepted.

4. Compute the invariant manifolds from the prior Lyapunov orbits by finding the eigenvalues and eigenvectors of their monodromy matrices in order to compute the initial conditions of the manifolds to introduce in the Runge-Kutta 7(8) solver of the non-linear Equations 6.
5. After having computed the invariant manifold orbits, the Poincaré maps on intersections between invariant manifolds are used to see if their profiles intersect, as presented in Section 2, meaning there are either a homoclinic or heteroclinic orbits.
6. If any intersection is found, a state vector of initial conditions is selected to be introduced again in the Runge-Kutta 7(8) integrator in order to propagate the orbit and see its path along the different manifolds.

4 Results and Discussion

As aforementioned in Section 1, the objective is to study the orbits within the stable and unstable invariant manifolds of Lagrange points L_1, L_2 and L_3 of the binary star Kepler 47 to find possible bound circumstellar or circumbinary orbits to be used as possible positions of exoplanets.

Since all the figures from this point forward are presented in dimensionless units, the following Table 1 gives a value for each of the units used.

Binary	μ	$M[M_{\odot}]$	$l[AU]$	$t[days]$
Kepler 47	0.2577	1.405	0.08	1.11

Table 1: Units for Kepler 47.

These values are taken from Jaime et al., 2014 considering the parameters of semi-major axis of the binary system as the distance between the stars (take into account that the eccentricities are close to zero therefore the semi-major axis can be considered the radius between the stars). The time unit has been calculated considering that the *gravitational constant* was dimensionalized to unit, therefore, using the values of the total mass and semi-major axis as units for mass and distance, the unit of time can be computed.

$$\begin{aligned}
&G = 6.67430 \cdot 10^{-11} m^3 kg^{-1} s^{-2} \\
&G = 3.96414 \cdot 10^{-14} AU^3 M_{\odot}^{-1} s^{-2} \\
&\bar{G} = 1 = G \cdot u_d^3 u_m^{-1} u_t^{-2} \\
&u_t = \sqrt{\frac{M}{Gl^3}}
\end{aligned} \tag{15}$$

where $\bar{G}$ is the unitary gravitational constant and u_d, u_m and u_t the units of distance, mass and time respectively.

In the following, we show the result of the different steps in the methodology applied to the binary star Kepler 47.

In Figure 6.a the Lyapunov orbits at the different libration points of Kepler 47 are displayed. See how the Lyapunov orbits are concentric and their size depends on the energy. As the invariant manifolds tend to or depart from those Lyapunov orbits, then, being the orbits concentric, their corresponding manifolds are embedded one inside the other, as can be seen in the projection in the $(x, \dot{x})$ plane in Figure 6.b for two of them. Note with the L_3 (rightmost) Lyapunovs that as the energy of the orbit not only increases the semi-major axis but loses its elliptic shape for a more oblated one at the sides facing the primaries. These represented Lyapunovs are for the ranges of Jacobi constant from $C = 3.2434$, corresponding to the larger L_3 Lyapunov, to $C = 3.5523$, corresponding to the most interior Lyapunov of L_1.

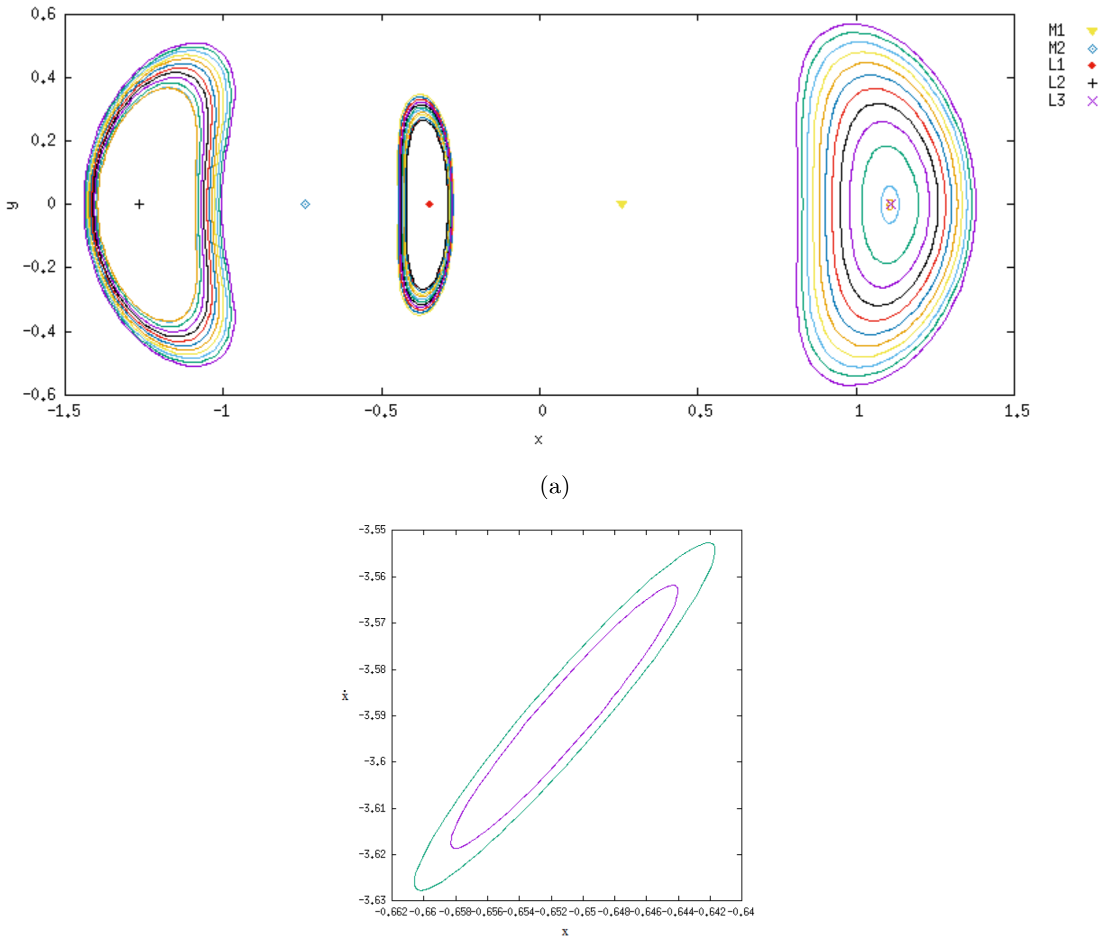

(a)

(b)

Figure 6: a) Lyapunov orbits around collinear points of Kepler 47. The ranges of Jacobi constants are between $C = 3.2434$ and $C = 3.5523$, for equal energy increments between orbits of each libration point of $1e-3$. See how the orbits lose their elliptical shape as energy (size) increases. The collinear points and the locations of the principals are represented, see how, as expected, L_1 and L_2 are closer to the smaller primary, denoted by M_2. b) Poincaré section for x and $\dot{x}$ of orbits of different level of energy. See how the orbits are concentric.

From these Lyapunov orbits, three are selected, one from each libration point so that they have the same energy and, for those orbits, the invariant manifolds are computed. This process consists on computing the initial conditions from the selected Lyapunov and then integrating the invariant manifold over time to obtain the four branches from each Lyapunov. As mentioned in Section 3, the integration is done with a Runge Kutta 7(8) method, with a tolerance of $1e-5$ in the energy disparities between the initial and the final energy, to ensure conservation, otherwise the orbit cannot be accepted.

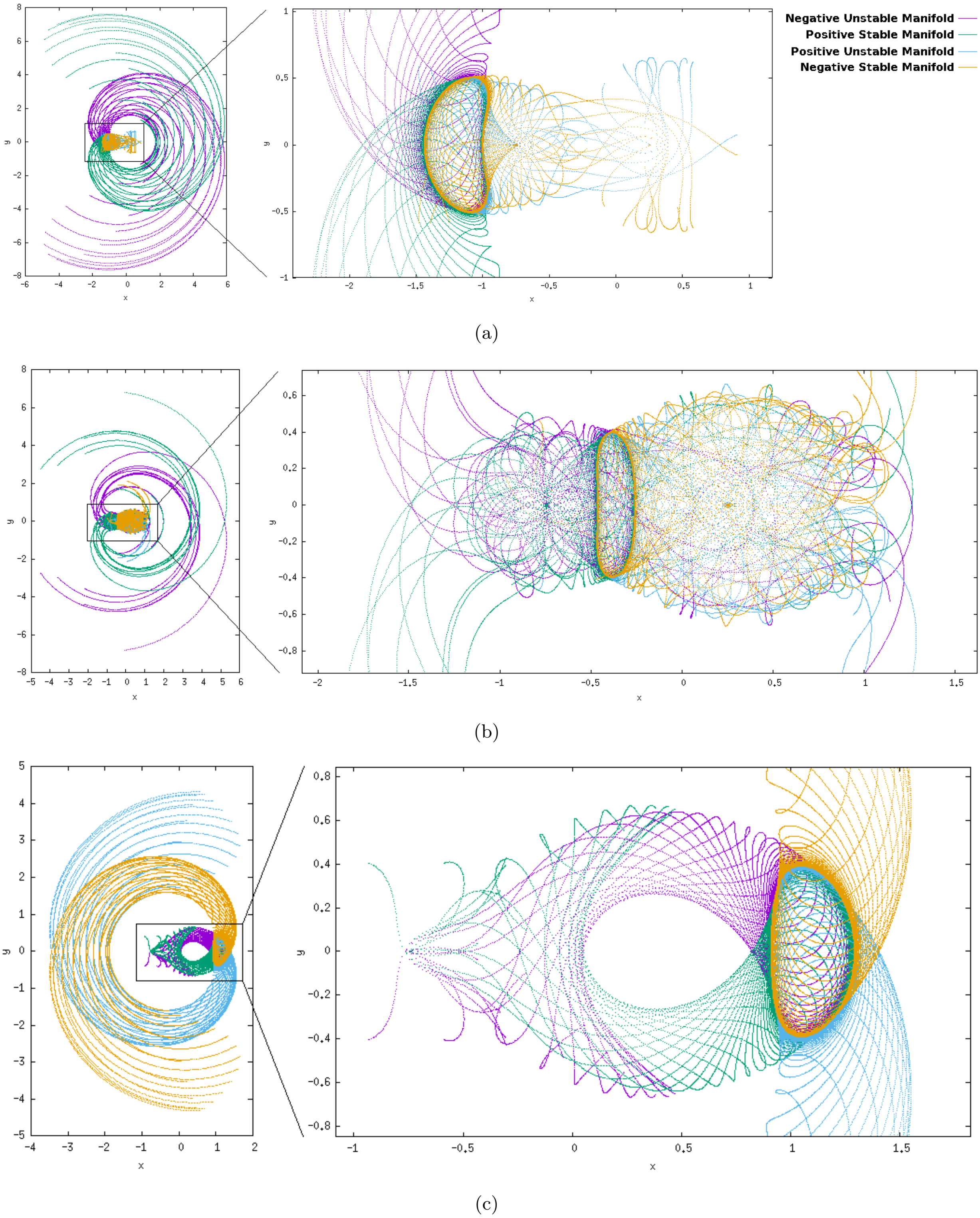

Figure 7: Invariant manifolds of the libration points of Kepler 47 for a Jacobi constant of $C = 3,3526$. The notation of *negative* or *positive* implies the direction of the initial conditions since for each manifold (stable or unstable) there are two possible directions. a) L_2 manifolds. b) L_1 manifolds. c) L_3 manifolds.

In Figure 7 the computed invariant manifolds from the Lyapunovs of Jacobi constant $C = 3,3526$ are presented. See how the manifolds depart from and tend to the Lyapunov they form perfectly its shape in its vicinities. It is interesting to note that in 7.b, where the L1 manifolds are represented, manifolds that should be restricted to the motion between L_1 and the other L_2 and L_3 points since it is the central point. Nonetheless it is seen how some of the orbits escape that region through those other points, this would only be possible if, as presented in Section 2, that orbit is part of the transit orbits of the manifolds of the other points. Therefore this could already point to the existence of heteroclinic orbits among manifolds of different libration points.

Figure 8 displays all manifolds together. In this figure it is possible to qualitatively see where the manifolds intersect in the configuration space, therefore, locations where they meet are used to represent their Poincaré sections to see if there are any intersections in phase space.

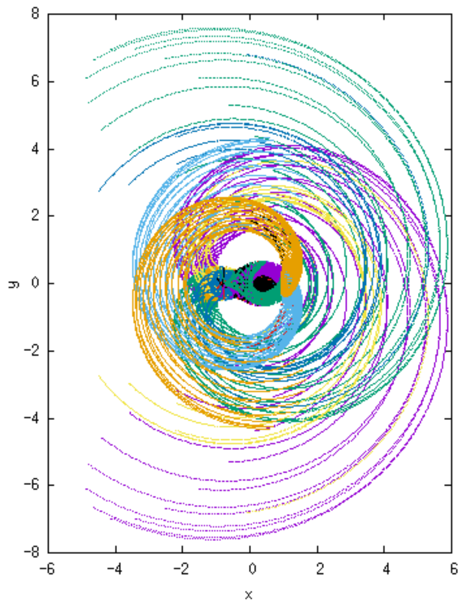

Figure 8: Manifolds from the Lyapunovs of Jacobi constant of $C = 3.3526$ for all libration points of Kepler 47.

Recall the different manifolds from Figure 7 and that they have a sense of motion depending whether they were stable or not, therefore, it is necessary that, in order for there to be an homoclinic or heteroclinic orbit, that the intersecting manifolds have the same direction. That is, for the manifolds between L_1 and L_2, the stable manifold of L_1 has to intersect with the unstable from L_2, otherwise the orbits would have different senses of motion. The same happens reciprocally and all intersecting manifolds, from the same and different Lyapunovs.

4.1 Homoclinic connections around L_3

Then, first the homoclinic connections are studied, for instance for the case of L_3 (Figure 7.c) two sections of $y = 0$ are used, for the intersections of all its manifolds, since it is seen that they meet on that plane. Figure 9 displays these sections. It is interesting to see in Figure 9 how there is an homoclinic connection only in the negative unstable and positive stable manifolds meaning that those homoclinic orbits would loop once around the larger primary and then spiral out through the other manifolds since they do not connect in order to close a global loop. This happens since, as metioned in Section 2, those orbits within the manifold tube in the phase space are *transit* orbits that go through *gate* of the libration point, i.e., enter the libration point region through a stable manifold and come out of it on the other side through an unstable manifold. This case will be studied propaganting an orbit with initial conditions as to be in that small region of the phase space of homoclinic orbits (see Figure 10).

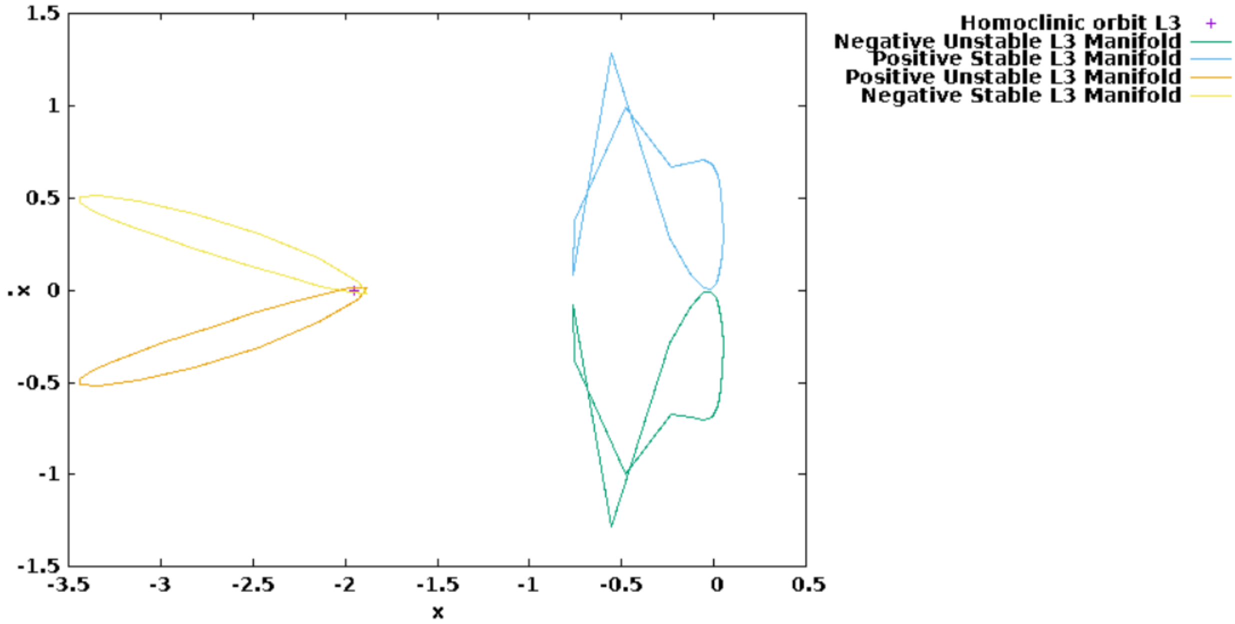

(a)

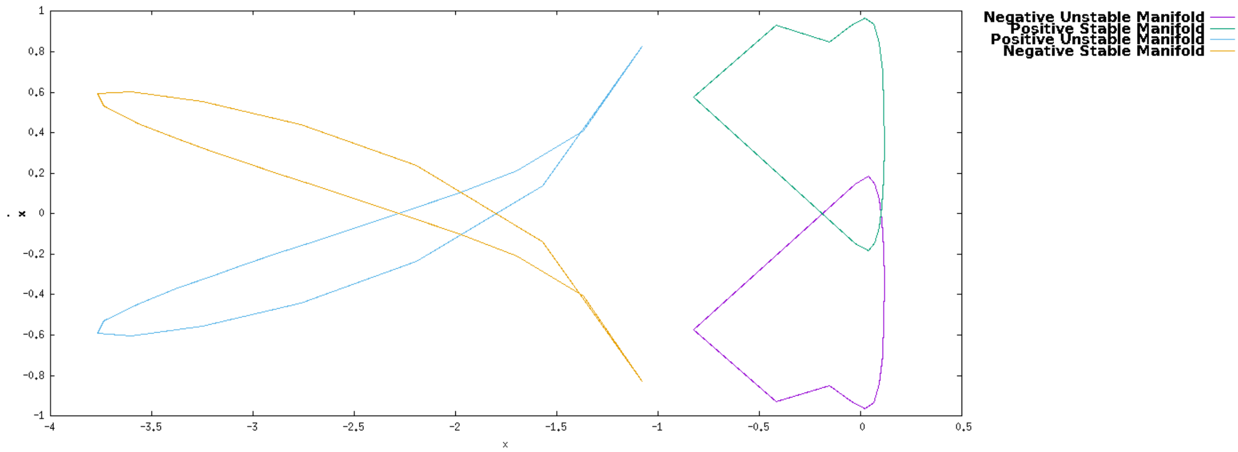

(b)

Figure 9: a) Poincaré map at $y = 0$ of manifolds arouns the L_3 libration point for a Jacobi constant $C = 3.3526$ of Kepler 47. See how for the inner manifolds there is a small region that overlaps. b) Same section at $y = 0$ but for a higher energy corresponding to a Jacobi constant of $C = 3.2435$. See how all sections overlap.

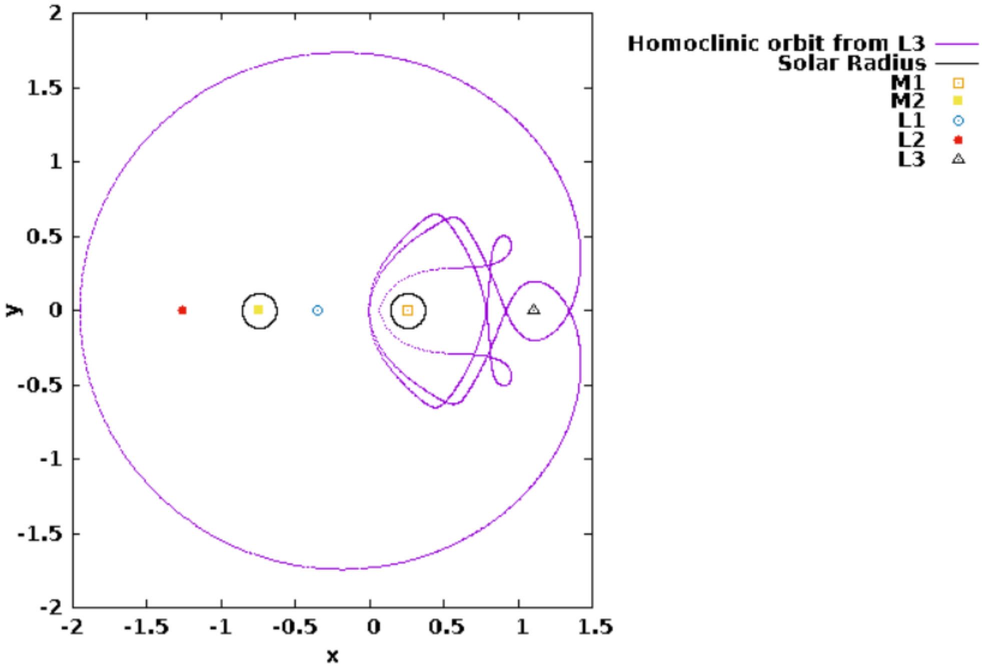

Figure 10: Trajectory of the homoclinic orbit with initial conditions within the prior intersection between manifolds from L_3 of Kepler 47 (Figure 9). Here the locations of the primaries and the libration points are also represented. The equivalent of a circle of solar radius is also represented on each primary to have an idea of the scale of the problem. It can be seen how the orbit loops in a circumbinary trajectory and enters through L_3 to move around m_1 in circumstellar loops.

Num. Orbit	x	y	$\dot{x}$	$\dot{y}$
1	-1.9500	0.0000	0.0000	-1.3193

Table 2: Initial conditions of the orbit propagated to find homoclinic orbits in L_3 manifolds.

All this trajectory has been computed using the initial condition in Table 2 and for a total time span of 16.145 time units, which, after looking the value for this unit for Kepler 47 in Table 1, represents 17,92 days, which is not a long period of time. This span has been used to avoid possible numerical dissipation due to error accumulation of long propagations.

Figure 9 shows how the positive unstable and negative stable manifolds do not connect by very little velocity difference, which would imply that for another energy there could exist also a connection between those two manifolds. That is because, as mentioned in Section 2 and can be seen in Figure 6.b, the manifolds are concentric among them as so are the Lyapunovs, therefore, for higher energies, the manifolds would be larger and there could be intersection, as displayed in Figure **??**, implying a possible periodic homoclinic orbit. That other scenario is not assessed though since the energy studied in this case is that of the Jacobi constant of 3.3526.

4.2 Homoclinic connections around L_2

Following the research for homoclinic connections between the manifolds, L_2 is assessed. For L_2 (Figure 7.a) the section of $y = 0$ is used for the crossing of the *negative unstable manifold* and the *positive stable manifold*, and the section $x = -0.655$ for the crossing of the *positive unstable manifold* and the *negative stable manifold*. In Figure 11 the results for L_2 are presented.

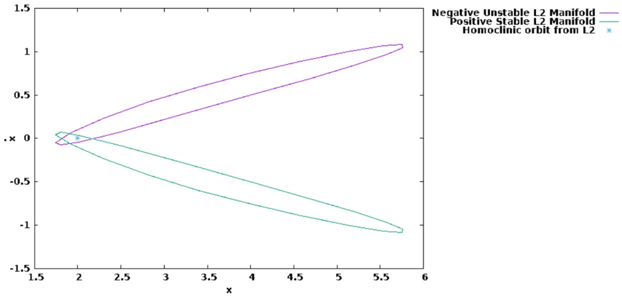

(a)

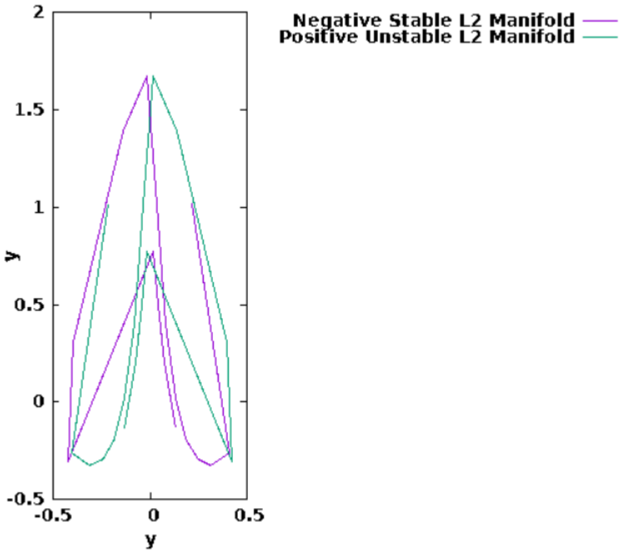

(b)

Figure 11: a) Poincaré map at $y = 0$ of negative unstable and positive stable manifolds around the L_2 libration point of Kepler 47. These manifolds also present overlapping where homoclinic connections can happen. The section of the candidate to be homoclinic orbit, that is later integrated, is also displayed. b) Poincaré map at $x = -0.655$ of positive unstable and negative stable manifolds around L_2 of Kepler 47.

Now it would be interesting to look for homoclinic orbits to see if in L_2 there could also exist a bound orbit, i.e., that does not leave the vicinity of the binary system. As with L_3, an initial condition (Table 3) satisfying the homoclinic connection of L_2 from Figure 11 is propagated and displayed in Figure 12. All these orbits are also integrated for 7.56 time units which are 8.39 days, which is again a really short period, but as long as is part of a bound orbit it can be a good candate.

Num. Orbit	x	y	$\dot{x}$	$\dot{y}$
1	2.0000	0.0000	0.0000	-1.3707

Table 3: Initial conditions of the orbit propagated to find homoclinic orbits in L_2 manifolds.

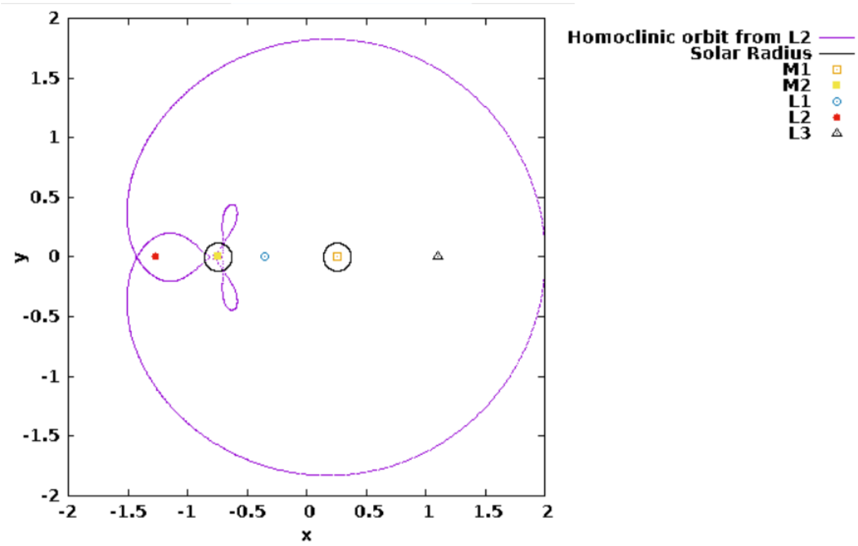

Figure 12: Trajectory of the set of orbits with initial conditions to find homoclinic orbits from L_2 on Kepler 47. The same behavior as in L_3 is obtained. Again, the span of the integration is limited to avoid numerical dissipation.

As it is said in Figure 12, the orbit has the same behavior as those studied for L_3, nonetheless in this case it becomes a trajectory of alimentation of the primary as can be seen how it enters the *solar radius*. Despite the fact that there is collision with the primary, this proves that **there can be trajectories bound in the binary system due to homoclinic connections between manifolds**.

4.3 Homoclinic connections around L_1

For L_1 the intersections of Figure 13 are found at $x = -0.75$ for the positive stable and negative unstable manifolds and at $x = 0.4$ for the positive unstable and negative stable manifolds.

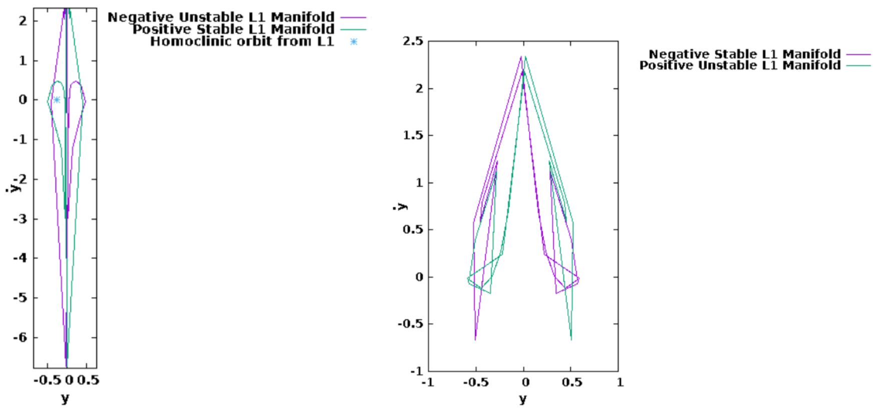

(a) (b)

Figure 13: These manifolds from L_1 of Kepler 47 also present regions of intersection. a) Poincaré map at $x = -0.75$ of negative unstable and positive stable manifolds around the L_1 libration point of Kepler 47. It also represents the section of the orbit integrated as candidate to be homoclinic. b) Poincaré map at $x = 0.4$ of positive unstable and negative stable manifolds around L_1 of Kepler 47.

Figure 14 presents the results of the propagation of an orbit within the homoclinic intersection of Figure 13 with the initial condition presented in Table 4. It is noticeable that the same behavior is found in general, that is, the trajectories in Kepler 47 are dominated by collision with the primaries due to the small distance between the primaries as seen in Table 1. It is important to see though, that in this case the orbit is not bounded, meaning that it transits through L_2 and L_3 and spirals away from the binary system. Therefore this orbit can not be homoclinic. Perhaps this fenomenon is caused because the orbit actually is not inside a region of connection among manifolds. Take into account that the sections of Figure 13 are not very precise due to the lack of manifold orbits, it would be necessary to have much more orbits in the invariant manifold to have it perfectly defined. Nonetheless, due to computational limitations only these few could be computed.

Num. Orbit	x	y	$\dot{x}$	$\dot{y}$
1	0.0000	-0.2500	1.3017	0.0000

Table 4: Initial conditions of the orbit propagated to find homoclinic orbits in L_1 manifolds.

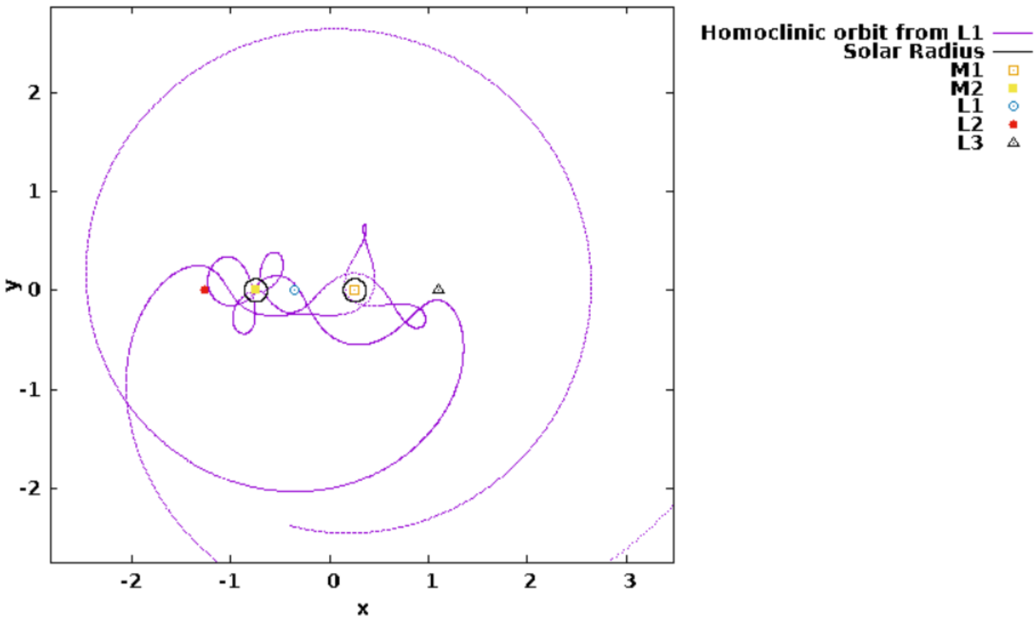

Figure 14: Trajectory of the orbit with initial condition presented in Table 4 to find homoclinic orbits from L_1 on Kepler 47. The same behavior as in L_2 is obtained, that is, the orbit collapses with the principal.

4.4 Heteroclinic connections

For these type of connections in Figure 15 are shown the intersections between the manifolds of L_1, L_2 and L_3.

Figure 15 represents the heteroclinic connections between all manifolds. Note that the Poincaré sections of the manifolds of L_1 and L_3 at $x = 0.4$ are symmetic. For this reason, for the other connections only one pair of branches is presented. See how intersections between L_2 and L_1 as between L_1 and L_3 present homoclinic orbits, while for L_2 and L_3 there are not. This coincides perfectly with the behavior seen in all integrated orbits, that as their trajectories can move between libration points without problem through those homoclinic and heteroclinic connections but, as soon as they enter one of this branches with a state vector that does not have homoclinic connection, there is no way of turning back since due to the absence of heteroclinic connection the orbit will spiral away from the binary irrevocably. Despite the effort of searching for heteroclinic orbit, no

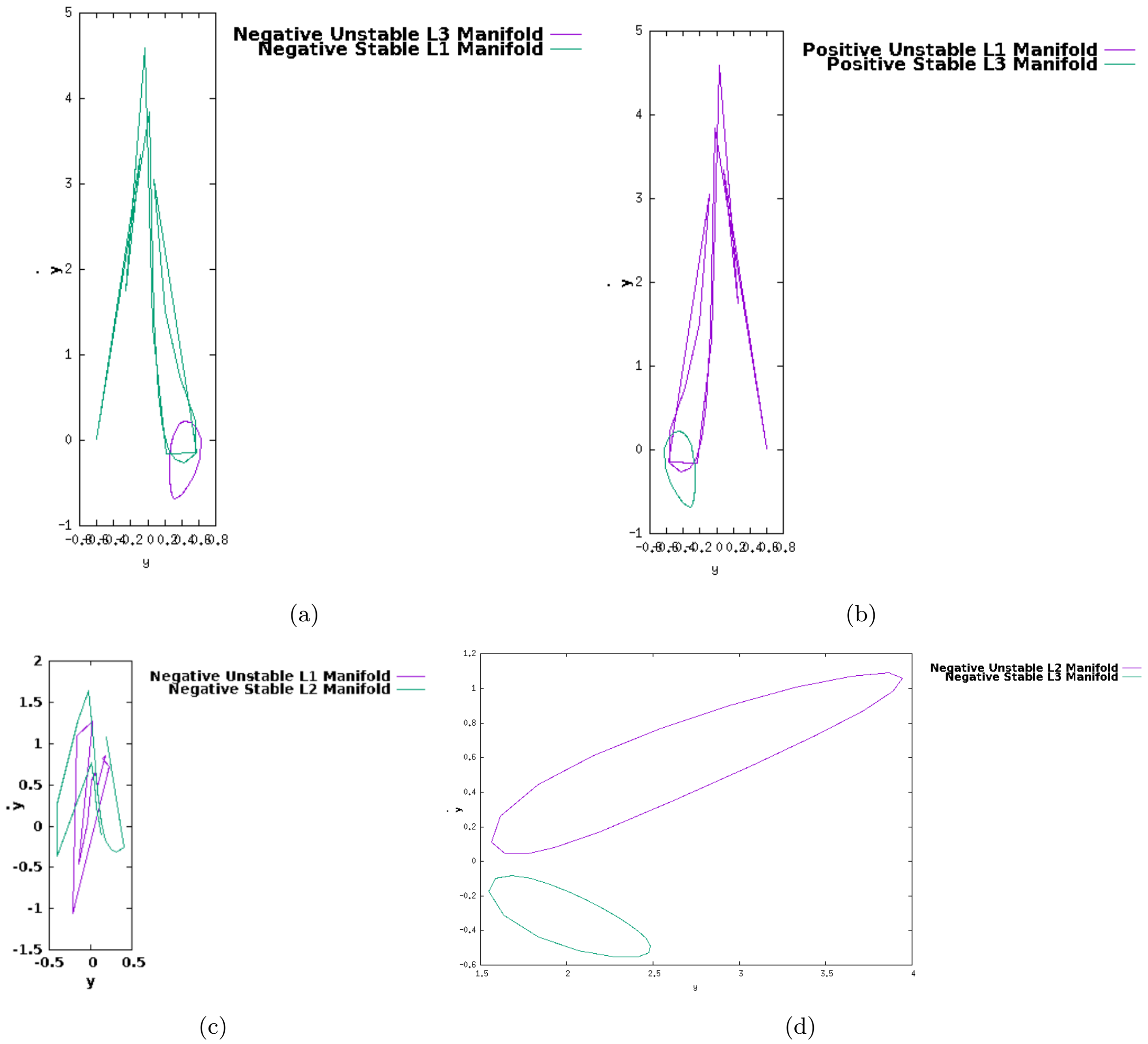

Figure 15: Intersections between all invariant manifolds. a) Intersection between L_1 negative stable manifold and L_3 negative unstable manifold at $x = 0.4$. b) Intersection between L_1 positive unstable manifold and L_3 positive stable manifold at $x = 0.4$. c) Intersection between L_1 negative unstable manifold and L_2 negative stable manifold at $x = -0.6$. d) Intersection between L_2 negative unstable manifold and L_3 negative stable manifold at $x = 0$.

real trajectories were found. Some bound orbits were found after propagating initial conditions but non of them seemed to be related to the invariant manifolds.

5 Conclusions

Fist, it is clear that sufficient homoclinic and heteroclinic connections have been seen in the case of Kepler 47 by studying only one value of Jacobi constant. Recall that in the Section **??** the assessment of the homoclinic connections for L_3 is done, where the differences due to a change in energy can be seen.

Then, even though there has not been found a specific orbit that can be considered as stable, i.e. bound to the vicinities of the binary, that does not collapse with the primary, the sighting of a pair of bound orbits at L_1 manifolds gives a glimpse of the possibility of there being an actual bound orbit that does not collapse. Perhaps that orbit would be at the same Jacobi constant but with slighlty different initial conditions or simply for another energy.

The main characterictic of the system that has influenced in the results, besides the mass parameter, has been the small distance between the stars, which has implied that most likely all the orbits of the invariant manifolds that form part of the heteroclinic orbit family, end up collapsing with either of the principals. Therefore for this binary, the motion between invariant manifolds has the effect of mainly transporting material into the stars as paths of cleaning the neighbouring regions and increasing their metallicity.

Overall it can be confirmed that homoclinic and heteroclinic orbits are present in this type of stellar system and that they can also constitute bound paths where, if the relative distances allow to it, planetary formation could occur.

6 Future Work

As has been seen, the study of the invariant manifolds indeed presents a possibility to the existance of bound orbits around the binary system. Nonetheless the work herein developed could be extended to study other energies of the same binary, Kepler 47, in order to find more possible connections. Despite that, this study could be extended as follows.

For those orbits confirmed to be bounded to the vicinities of the binaries, i.e. they do not spiral away to infinity, it would be interesting to convert the coordinates to the initial frame first and then to the set of coordinates used for astronomical observation so that the projection of the orbit is obtained as it would be seen from Earth. This way it would be possible to have a region in the sky where to look at in order to find the possible exoplanets laying in the orbit.

A different approach to the investigation would be, since certain binary systems are known to contain exoplanets, instead of looking for connections among invariant manifolds in general, see whether the orbits of these known planets correspond to any invariant manifold trajectory. That is, finding a valid state vector of the planet to use as initial conditions for the numerical integration of the orbits and then checking if they are within the invariant manifolds of their same energy. Kepler 47 would be a good candidate since it has three known planets.

Extend the *Circular Restricted Three Body Problem* to the *General Restricted Three Body Problem* to take into account binaries with eccentricities, following this way the line of the study of Jaime et al., 2014, where not only circular binaries are considered (which is a clear restriction since most of the systems are not circular) but also excentrical systems are taken into account, which expands the pool of possibilities.

References

Jaime, L. G., Aguilar, L., & Pichardo, B. (2014). Habitable zones with stable orbits for planets around binary systems., *443*(1), 260–274. https://doi.org/10.1093/mnras/stu1052

Pichardo, B., Sparke, L. S., & Aguilar, L. A. (2005). Circumstellar and circumbinary discs in eccentric stellar binaries., *359*(2), 521–530. https://doi.org/10.1111/j.1365-2966.2005.08905.x

Szebehely, V. (1967). *Theory of orbits. The restricted problem of three bodies.*

Koon, W., Lo, M., Marsden, J., & Ross, S. (2011). *Dynamical Systems, the Three-Body Problem and Space Mission Design*. Marsden Books.

Romero-Gómez, M., Masdemont, J. J., Athanassoula, E., & García-Gómez, C. (2006). The origin of rR_1 ring structures in barred galaxies., *453*(1), 39–45. https://doi.org/10.1051/0004-6361:20054653

Koon, W. S., Lo, M. W., Marsden, J. E., & Ross, S. D. (2000). Heteroclinic connections between periodic orbits and resonance transitions in celestial mechanics. *Chaos*, *10*(2), 427–469. https://doi.org/10.1063/1.166509

Romero-Gomez, M., Athanassoula, E., Masdemont, J. J., & Garcia-Gomez, C. (2007). The formation of spiral arms and rings in barred galaxies. *arXiv e-prints*, Article arXiv:0712.4391, arXiv:0712.4391. https://doi.org/10.48550/arXiv.0712.4391